Microphase Separation of Block Copolymer Thin Films

Jilin Zhang, Xinhong Yu, Ping Yang, Juan Peng, Chunxia Luo, Weihuan Huang, Yanchun Han*

Today, high-ordered micro- and nano-patterned surfaces are widely used in many areas, such as in the preparation of super-thin dielectric films, photonic crystals, antireflective films, super-non-wetting surfaces, bio-compatible surfaces and microelectric devices. Considering the critical fabrication conditions and the irreducible high cost of the photolithography technique in patterning nano-scale structures (<100 nm), the development of other micro- and nano-patterning techniques that can be used to fabricate long-range ordered features – especially nanoscale arrays – is a promising subject in surface science. In contrast to the traditional photolithography patterning technique, block copolymers can spontaneously phase separate into arrays of periodic patterns with length-scales of 10–50 nm, which provides an efficient pathway to pattern nanoscale features. Today, preparing long-range ordered arrays by block copolymer microphase separation is one of the most promising techniques for the fabrication of nanoscale arrays, not only being a simple process but also having a lower cost than traditional methods. In this feature article, we first summarize the many techniques developed to induce ordering in the microphase separation of the block copolymer thin films. Then, evolution, order–order transitions and reversible switching microdomains are considered, since they are very important in the ordered engineering of microphase separation of the block copolymer thin films. Finally, the outlook of this research area will be given.

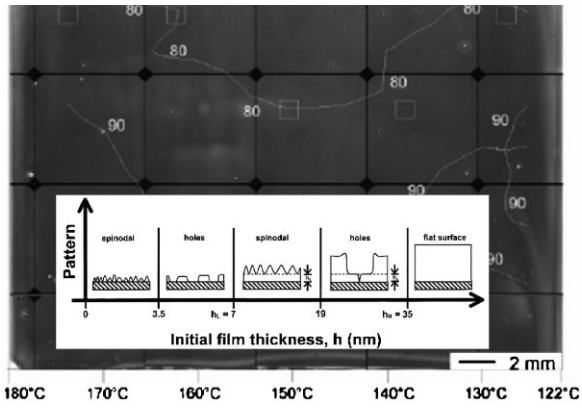

Introduction

Well-ordered micro- and nano-structured surfaces are of great interest in many areas, as they can be applied as catalysts, photonic band-gap materials, optical stop-bands, sensors, microreactors, combinatorial arrays, microelectromechanical systems (MEMS), and microanalytical systems. Today, traditional UV photolithography[1,2] can produce surface features in high resolution at scales of less than 40 nm with remarkable speed and efficiency, the cumulative result of decades of engineering refinements.

J. Zhang, X. Yu, P. Yang, C. Luo, W. Huang, Y. Han
State Key Laboratory of Polymer Physics and Chemistry, Changchun Institute of Applied Chemistry, Chinese Academy of Sciences; Graduate University of the Chinese Academy of Sciences, 5625 Renmin Street, Changchun 130022, P. R. China
Fax: +86 431-85262126; E-mail: ychan@ciac.jl.cn
J. Peng
The Key Laboratory of Molecular Engineering of Polymers, Ministry of Education, Department of Macromolecular Science, Fudan University, Shanghai 200433, China

DOI: 10.1002/marc.200900541

However, the cost for these improvements and the critical fabrication conditions restrict growth unavoidably, especially in patterning nanofeatures. Given current understanding, it is not anticipated that state-of-the-art 193 nm immersion lithography can be extended beyond the 22 nm node.[3,4] Thus, prospective replacement technologies – such as extreme UV lithography and nano-imprint lithography – have emerged. These alternatives still face some significant technical hurdles and so it is difficult to predict their future in the fabrication of micro-/nano-devices.

Microphase separation of block copolymers (BCPs) can, in principle, provide arrays of periodic patterns with length-scales of 10–50 nm, via a simple and low-cost process.[5] In contrast to the traditional lithography technique, microphase separation of the BCP thin films has two main advantages. Firstly, it is easier on the fabrication process equipment, and also more robust since the patterned polymer surfaces can be used as models to pattern other organic and inorganic surfaces, which cannot be patterned directly in the fabrication of micro-optoelectronic devices. Secondly, phase-separated polymer surfaces have many special applications in multi-disciplinary research, such as organic/bio-molecule purification, separation and adsorption by porous polymer films,[6] drug portability and delivery,[7] and low-dielectric-constant microelectric devices,[8] etc. Therefore, polymer phase separation is considered to be a promising pathway towards microfabrication of specific size and surface compositional patterns in polymer science. In this feature article, we will summarize the progress of designing well-ordered microphase separation features in BCP thin films, which is a simple and convenient technique in the fabrication of nanoscale arrays.

Usually, microphase separation features of the BCP thin films depend on some traditional parameters, such as segregation strength (χN),[9–16] film thickness (d),[17] annealing temperature (T)[18] and substrate (Sub),[17] etc. However, the nanofeatures controlled by these traditional parameters are usually lacking of good order, which restricts their applications in patterning. Therefore, obtaining high-ordered microphase separation arrays is the most important issue in researching BCP microphase separation. In the following section, we will summarize some orientation techniques, which are promising for the achievement of high-ordered nano-features.

Ordered Engineering of Microphase Separation of BCP Thin Films

Thermal Annealing and Temperature Gradient

In a disordered BCP system, when the segregation strength (χN) is above ≈10.5 – a critical value for BCPs – the disordered system tends to phase-separate into an "ordered" state.[19,20] This transition is termed an order–disorder transition (ODT), and the transition temperature at which point this phase transition occurs is designated the order–disorder transition temperature (T_d). For a given BCP system, since χ is dependent on the temperature and gradually decreases with the external temperature (T), thermal-annealing is efficient in inducing the microphase separation of BCPs.

In a BCP thin film, the microphase separation feature is strictly governed by the film thickness (d) during the thermal annealing. Limary and Green[18] researched a series of symmetric polystyrene-*block*-poly(methyl methacrylate) (PS-*b*-PMMA) thin films having different thickness and microphase separation above T_d. They found films dewetted on the silicon substrate, and formed bi-continuous spinodal-like patterns when the film thickness was below 3.5 nm ($d < 3.5$ nm). With the film thickness increasing to the range of 3.5 nm $< d <$ 7 nm (d_L), discrete holes appeared randomly throughout the film. When the film thickness increased to the range 7 nm $< d <$ 35 nm (d_H), autophobic behavior occurred in the film, whereby the top layer of thickness ($d - d_L$) dewetted a dense "brush" of ordered copolymer of height d_L anchored to the silicon substrate. Figure 1 shows the final surface features as a function of the initial film thickness after thermo-annealing,[18] which includes a bi-continuous spinodal pattern ($d_L < d <$ 19 nm), discrete holes (19 nm $< d < d_H$), and stable smooth films when d exceeds 35 nm.

From Limary and Green's point-to-point research,[18] the relationship between BCP microdomains and the film thickness was discovered in part, when the thin films were annealed above T_d. However, the microphase separation of BCP thin films is a complex phenomenon and the relevant parameter space is rather large, including the chain length, etc. To avoid the hard process of fabricating a large number of different BCP films with different thicknesses, Smith et al.[21] ingeniously prepared a series of grad-thick symmetric PS-*b*-PMMA thin films with varying molecular mass (M) (Figure 2, top), and thermo-annealed the samples in a temperature gradient, which was orthogonal to the thickness-gradient direction (Figure 2, bottom). In contrast

Yanchun Han received her B. S. degree in polymer science from the University of Science and Technology of China (USTC) in 1990 and her Ph. D. from the Changchun Institute of Applied Chemistry, Chinese Academy of Sciences (CIAC) in 1995. She is now a professor at the State Key Laboratory of Polymer Physics and Chemistry in CIAC. Her research interest includes organic optoelectronic devices, polymer films, surfaces and interfaces, and nanostructured composite materials.

Macromol. Rapid Commun. **2010**, *31*, 591–608

Macromolecular Journals
DOI: 10.1002/marc.200900541

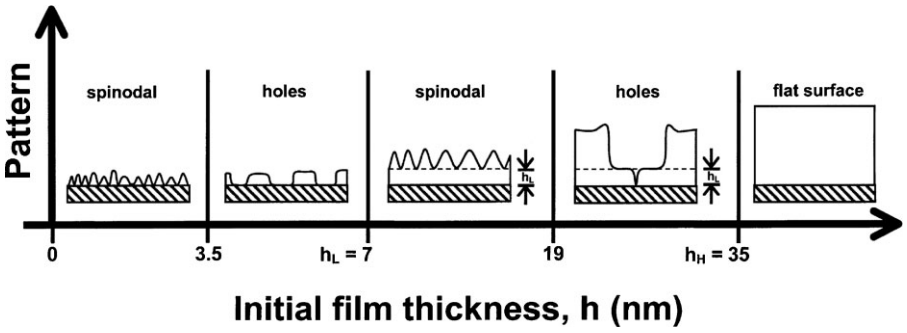

Figure 1. Surface feature as a function of initial film thicknesses in PS-*b*-PMMA diblock copolymer. These films were annealed at 170 °C, a temperature above the T_d. The topography of the films prior to annealing is flat.[18] Copyright 1999 American Chemical Society. Reproduced with permission.

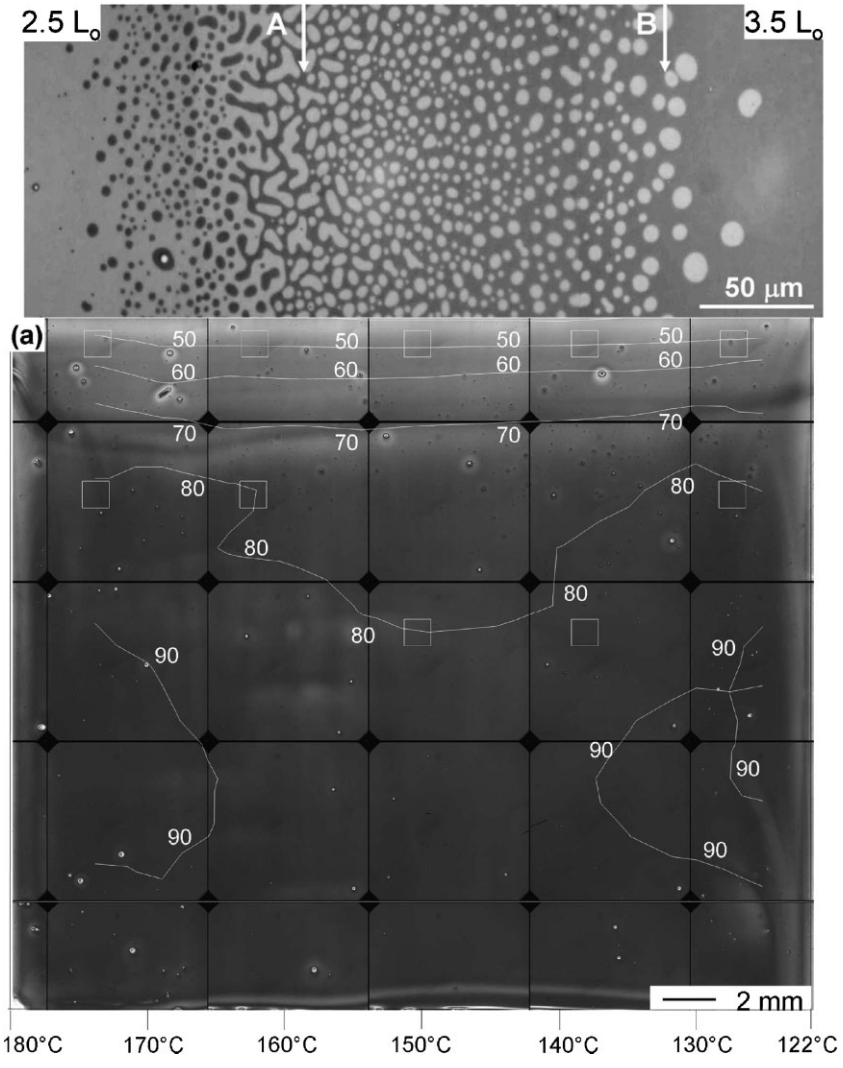

Figure 2. Top: Optical micrograph obtained from a block copolymer thin film gradient that varies from 2.5 Lo to 3.5 Lo, where Lo is a lamellar period. Arrows designate the approximate locations of: A) 53 nm film, and, B) 80 nm film along this continuous morphology variation. Bottom: a temperature (*T*) gradient orthogonal to the thickness-gradient PS-*b*-PMMA film.[21] Copyright 2007 American Chemical Society. Reproduced with permission.

to the microdomains at the different points, a series of relationships between microphase separation features and the film thickness (*d*), annealing temperature (*T*), annealing time (*t*) and the molecular mass (*M*) were discovered, which might be incorporated into a proposed theory of pattern formation in generic lamellae-forming films.

Furthermore, temperature-gradient heating (also called "zone heating") can be employed to orient the microdomains of the BCP thin films, which was firstly performed by Hashimoto et al.[22,23] They achieved the orientation of the lamellar microdomains in a PS-*block*-poly(isoprene) (PS-*b*-PI) BCP thick film via annealing in a temperature gradient. Subsequently, Berry et al.[24] applied a temperature gradient to anneal thin films of PS-*b*-PMMA. Their results showed that the defect density of the cylindrical microdomains in PS-*b*-PMMA thin films decreased significantly with decreasing velocity under a given temperature and temperature gradient (Figure 3). Recently, Hashimoto et al.[25] applied a moving temperature gradient field to the BCP, forming a hexagonally-packed cylindrical (hex-cyl) microdomain which developed into unique columnar grains macroscopically extended along the gradient axis. They found both the cylinder axis and the (100) plane of the hex-cyl microdomain were normal to the gradient axis, and the rotational angle of the cylinder around the gradient axis was fixed. However, by tilting the glass substrate at an angle of 45° with the

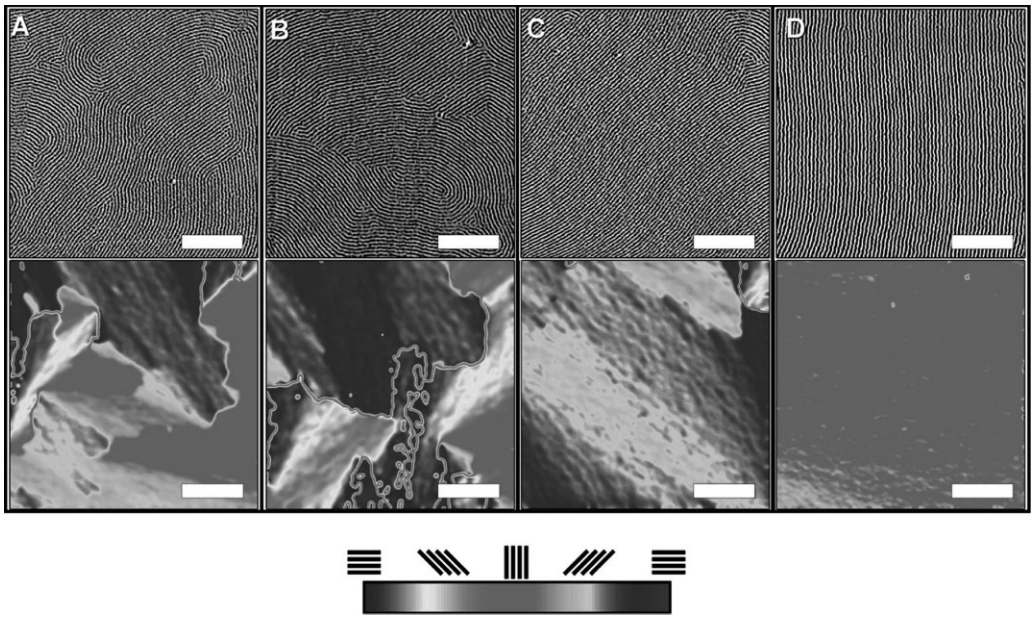

Figure 3. AFM phase images and cylinder orientation maps of PS-b-PMMA thin films annealed with push velocities of a) 100, b) 40, c) 5, and, d) 1 $\mu m \cdot s^{-1}$.[24] Copyright 2007 American Chemical Society. Reproduced with permission.

respect to the gradient direction, the moving temperature gradient itself could create the columnar grain feature without any dependence on the glass surface-induced ordering effect, which meant the moving temperature gradient field became the dominant effect over those of the glass surface-induced field.[26] At present, temperature-gradient annealing remains a potential technique to create highly ordered microdomains over a large area, which is deeply, but not solely, governed by the uniformity and the gradient value of the applied temperature gradient and the annealing time.

Solvent–Vapor Annealing

Thermal annealing is a common method used to induce microphase separation in BCP thin films when the molecular mass of the BCP is not excessively high. However, if the polymerization degree (N) of the BCP is too large, the order–disorder transition temperature (T_d) increases greatly. Thus, the thermal annealing method is not as efficient for a high molecular weight BCP as on a lower molecular weight counterpart. At this time, solvent-vapor annealing has been proven in experiments to be another efficient method to induce microphase separation with long-range order in BCP thin films.[27–36] For example, Kim et al.[36] annealed PS-*block*-poly(ethylene oxide) (PEO) thin films in an atmosphere containing benzene vapor for 48 h, which greatly reduced the formation of defects and yielded arrays of cylindrical microdomains with long-range lateral order in the film.

When an amorphous BCP thin film is exposed to a solvent vapor, the surface absorbs a monolayer of solvent molecules, which changes the film boundary condition in the air. Moreover, each solvent vapor has a different selectivity to the segments of the BCPs; correspondingly, the microphase separation features are strictly dependent on the selectivity of the solvent vapors. For example, Peng et al.[37] studied the microdomains of symmetric PS-*b*-PMMA thin films after annealing the films in several solvent vapors having different selectivities (Figure 4). Upon neutral tetrahydrofuran (THF) vapor annealing, in which PS and PMMA showed an equal degree of swelling, the film showed terraced features (surface-parallel lamellae). Upon PS-selective CS_2 vapor annealing, the PMMA block formed aggregates, while the PS block surrounded the PMMA aggregates as a shield to avoid the unfavorable PMMA-solvent contact. Finally, upon strong PMMA-selective acetone vapor annealing, the strong tendency of acetone molecules to swell the PMMA blocks yielded the uprising of the PMMA blocks and destabilized the film to the point of dewetting. The uprising PMMA block perforated the upper PS-rich layer at the nanoscale and migrated to the surface in a hexagonal array, as a response to the acetone attraction. As is well know, the thin-film morphology is determined to a large extent by the competition between the mobilities of the PS and PMMA blocks, which are influenced by the degree of swelling of the polymer films. In the case of a higher PMMA degree of swelling, the driving force that attracts the PMMA block upward is stronger. Therefore, the PMMA block perforates the PS-rich layer directly and migrates to the surface, resulting in a

Macromolecular Journals
DOI: 10.1002/marc.200900541

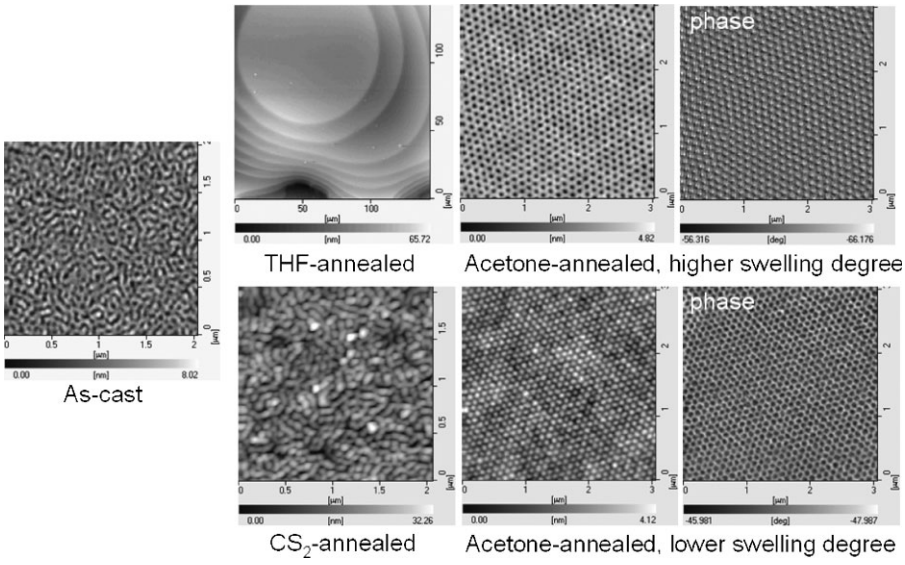

Figure 4. AFM images of symmetrical PS-*b*-PMMA film morphology after annealing in different solvent vapors.[37] Copyright 2006 American Institute of Physics. Reproduced with permission.

hexagonal array of depressions. On the other hand, in the case of a lower PMMA degree of swelling, the attraction of PMMA by acetone vapor is relatively weaker and therefore the aggregation of PS blocks dominates. The PS blocks aggregate to form spherical cores to avoid the contact to acetone, and the PMMA blocks form a layer around the PS cores, resulting in an array of spheres.

Orientation of Microphase Separation by Control of Crystallization

Crystallization can induce the orientation of microdomains in semi-crystalline BCPs, which is usually combined with other techniques, such as oscillatory shear, wetting–dewetting, and epitaxy, etc.[38] For example, in semi-crystalline BCPs, oscillatory shear can induce the molecule chain orientation of the confined crystals in the BCP microdomains.[39–45] Cheng et al. studied the oscillatory shear induced orientation of the crystalline PEO block, forming microphase separated lamellar,[41] cylindrical[42] and hexagonally perforated arrays[43–45] in PS-*b*-PEO BCP systems. They found the chain orientation of the PEO block depends on the crystallization rate (or crystallization temperature); that is, with a fast crystallization rate (low crystallization temperature), the orientation was random; otherwise, the chain axis of the PEO block was configured parallel to the surface normal of the microphase-separated domains when the crystallization rate was slow (e.g., crystallization during high-temperature annealing).

Wetting–dewetting of BCP thin films can be used to influence the microdomain orientation when also combined with crystallization in semi-crystalline BCPs.[46,47] For crystal growth rates higher than $1\,nm \cdot s^{-1}$ in a microphase-separated structure, a lamellar microdomain structure perpendicular to a non-crystalline silicone oxide substrate was found in a thin film of hydrogenated polybutadiene (PB) (amorphous)/PEO (semi-crystalline) BCP[47] (Figure 5, left). Moreover, the crystallization of the PEO block occurred at wetting–dewetting boundaries, such as three-phase contact lines generating lateral alignment of the perpendicular lamellae over a short distance.

Epitaxy, which is defined as the growth of a crystal of one phase on the surface of that of another phase in one or more strictly defined crystallographic orientations, can also be used to influence the microdomain orientation when combined with crystallization in semi-crystalline BCPs.[48–50] In epitaxial growth, a crystallizable solvent, such as benzoic acid, serves as a solvent for a semi-crystalline BCP when the temperature is above the melting point (T_m) of the solvent and becomes a substrate onto which the crystallizable block can orient when the block is cooled below the solvent's melting point. Using epitaxy to control the spatial and orientational order of BCP microdomains was initially introduced by de Rosa et al. They used epitaxy to control the molecular and micro-domain orientation of a poly(ethylene)-*block*-poly(ethylene propylene)-*block*-polyethylene (PE/PEP/PE) semi-crystalline tri-BCP thin film[51] (Figure 5, right). In order to apply this technique to BCPs, the semi-crystalline BCPs need to have at least one crystalline block capable of interacting with the solvent crystalline surface. At this time, epitaxy between a crystalline block and a crystalline substrate has been shown

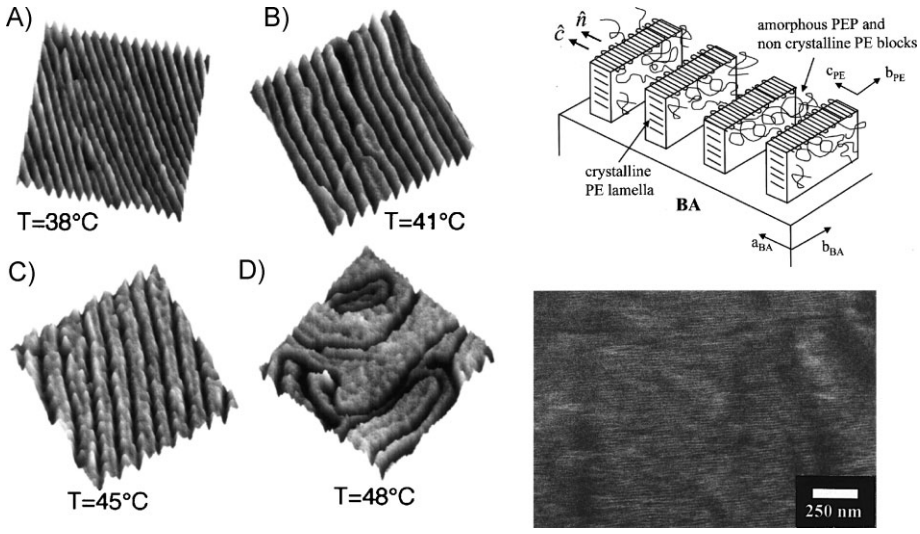

Figure 5. Left: AFM phase images from thin di-BCP films crystallized at different temperatures. The size of the images is 400 × 400 nm².[47] Copyright 1999 American Physical Society. Reproduced with permission. Top right: Schematic model showing the crystalline and amorphous microdomains in the PE/PEP/PE block copolymer epitaxially crystallized onto BA. Epitaxial relationship shows the relative orientation of the polyethylene lamellae on the benzoic acid. (100)PE//(001)BA, cPE//aBA and bPE//bBA. Bottom right: TEM (110) dark field image of a thin film of PE/PEP/PE BCP epitaxially crystallized onto BA crystal. The bright regions correspond to the crystalline PE lamellae in the Bragg condition.[51] Copyright 2000 American Chemical Society. Reproduced with permission.

to be an excellent approach to form highly aligned edge-on crystalline lamellae in both lamellar and cylindrical microdomains formed from semi-crystalline BCPs.

Orientation of Microphase Separation by Template Guiding

Graphoepitaxy

Graphoepitaxy (also called template guiding), which supplies a topographic confinement to the BCP thin films, is a simple and convenient method to induce well-ordered microphase separation features. Kramer et al.[52] first performed this technique by using topographically patterned substrates, which were fabricated by photolithography and chemical etching. Recently, it has been found that the wetting properties of the bottom and sidewalls of the trench, trough or well can govern the alignment orientation of the lamellar micro-domains in microphase separation. For example, Park et al.[53] found that when the bottom surface of the trench was neutral to both PS and PMMA micro-domains, in addition to a sidewall which was selective to one of the blocks, a parallel orientation of lamellar micro-domains could form on the selective sidewall surface, while a neutral sidewall gave a perpendicular orientation (Figure 6, top left). Cheng et al.[54] documented that this parallel orientation of lamellar microdomains to the sidewalls can also be achieved under non-equilibrium conditions, by using a BCP hybrid containing an organosilicate. Very recently, Park et al.[55] used two levels of topographical guiding patterns to register the microdomains of PS-*b*-PMMA lamella and found that the film thickness at the vertical face of the guiding patterns was the key parameter for ordered structures, while the difference between surface tensions of the two blocks provided an energetic mechanism for precise registration of the lamellae (Figure 6, top right).

Besides controlling the selectivity of sidewalls, prepatterned substrates can also induce well-ordered microdomains. Kim et al.[56] recently observed that perpendicular lamellae orient across the lines, yielding a crossbar nanostructure with self-assembled lamellae of approximately 20 nm half-pitched by using a grating of lines produced lithographically on a substrate. Since this perpendicular lamella alignment is energetically invariant to translation of the microdomains parallel to the ridges, precise registration of the microdomains relative to the guiding patterns is difficult (Figure 6, bottom left).

These microphase separation features prepared via template guiding can be used to array metals or semiconductors. Recently, Jeong et al.[57] used the soft graphoepitaxy method to prepare a serious of ordered sub-30 nm scale microphase separation morphologies (surface perpendicular or parallel lamellar or cylinder, vertical hexagonal cylinder and concentric cylinder) by self-assembling PS-*b*-PMMA thin films under a disposable topographic confinement. The ordered microphase separation features provided an efficient and scalable route to various functional nanostructures, such as metal and semiconductor nanowire arrays (Figure 6, bottom right).

Macromol. Rapid Commun. **2010**, *31*, 591–608

Macromolecular Journals
DOI: 10.1002/marc.200900541

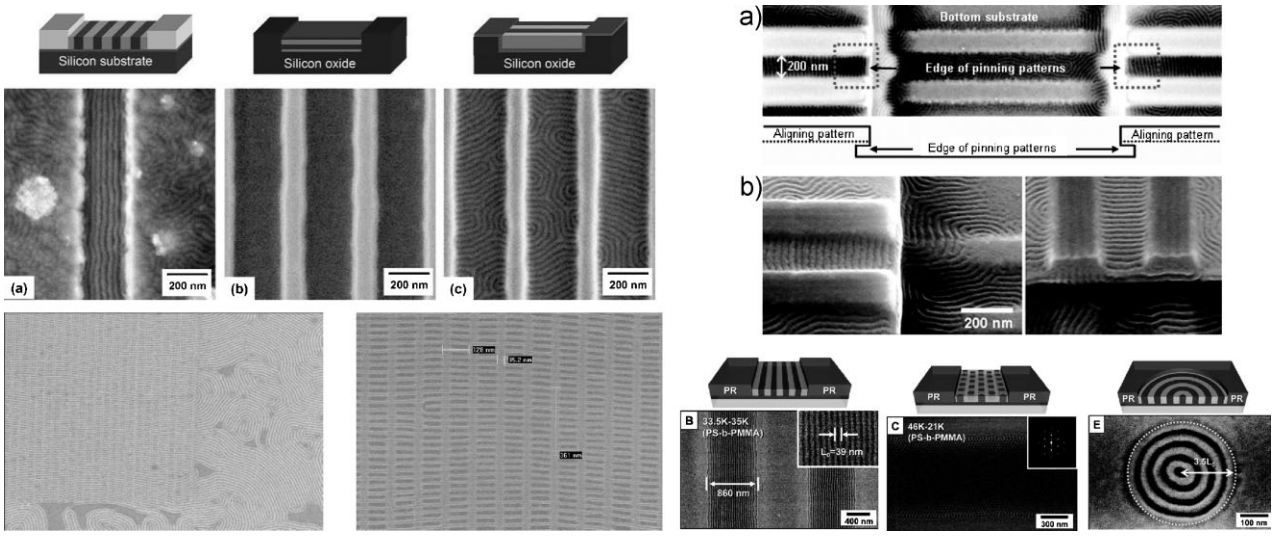

Figure 6. Top left: Lamellar microdomains of PS-*b*-PMMA on topographically patterened substrates. a) Gold (PS selective) sidewalls and neutral bottom, b) SiO_2 substrate, and, c) neutral sidewalls and bottom.[53] Copyright 2007 Wiley-VCH Verlag GmbH & Co. KGaA. Reproduced with permission. Bottom left: SEM image of the lamellae on a substrate containing corrugated patterns. The horizontal and vertical lines are lamellae and substrate corrugation from e-beam lithography, respectively.[56] Copyright 2008 Institute of Physics. Reproduced with permission. Top right: AFM images and Monte Carlo simulations of lamellae-forming block copolymer thin films on a substrate similar to the experiment.[55] Copyright 2009 American Chemical Society. Reproduced with permission. Bottom right: SEM images of oriented microdomains by soft graphoepitaxy.[57] Copyright 2009 American Chemical Society. Reproduced with permission.

Directional Casting

Guiding the direction of solvent evaporation would lead the solvent to have an orienting flow within a droplet of the BCP solutions, due to convection;[58,59] the BCP depositing from the droplet will then tend to phase-separate in an oriented manner. Therefore, directional casting is also an efficient technique to create ordered BCP microdomains. Kimura et al.[60] obtained highly oriented arrays of cylindrical microdomains of PS-*b*-PB by using the flow of a pinned solution droplet on a tilted substrate coupled with solvent evaporation. Due to a strong "bottom-to-top" directional flow of the solvent, the microphase separation of PS-*b*-PB is highly oriented, and the ordered feature is over tens of microns (Figure 7, left). Subsequently, Tang et al.[61] evolved this technique by using a flat nozzle (equipping a syringe) onto a moving substrate. By controlling the substrate's moving speed and the evaporation temperature, poly(*n*-butyl acrylate)-*block*-polyacrylonitrile (PBA-*b*-PAN) di-BCP could not only have an oriented microphase separation feature, but also various film thicknesses from 100 nm to 1 μm (Figure 7, right). Besides the film thickness, the size and the separation distance of the oriented micro-domains are also controllable in this technique. Kim et al.[62] produced highly ordered arrays of cylindrical micro-domains in a PS-*b*-PEO BCP thin film by using unidirectional solvent evaporation, from which a directed feature in the film was produced. They found the size and separation distance of the microdomains were controllable by using the co-solvents, which evidently extended the flexibility of the process.

Chemical Pattern Guiding

Similar to physical template guiding (graphoepitaxy), chemical template guiding is another efficient approach to align BCP microdomains: BCP microdomains can be oriented via control of the chemical heterogeneity on the substrate. In theory, a well guided alignment would suggest the length scale of the surface chemistry heterogeneity would be approximate to that of the micro-domain periodicity. In experiments, Rockford et al.[63] used a chemically striped (oxide and metal) substrate, on which the stripe width was comparable to the size of a polymer molecule. They distinctly observed that the alignment degree of micro-domains was a function of the degree of commensurability (δ: the ratio of the BCP period in the bulk to the substrate structure period). It was found that the lamellae were oriented normally to the substrate surface and directed by the underlying strips on the heterogeneous surface.

Performed with extreme UV interferometric lithography (EUV-IL), chemical template guiding can be used to prepare long-range defect-free BCP nano-features. Nealey et al.[64,65] achieved long-range defect-free alignments of PS-*b*-PMMA lamellar micro-domains by using the directed self-assembly technique combined with EUV-IL. In their experiments, the patterns of chemical contrast were prepared in two steps: i) preparation of a thin monolayer of polymer brush

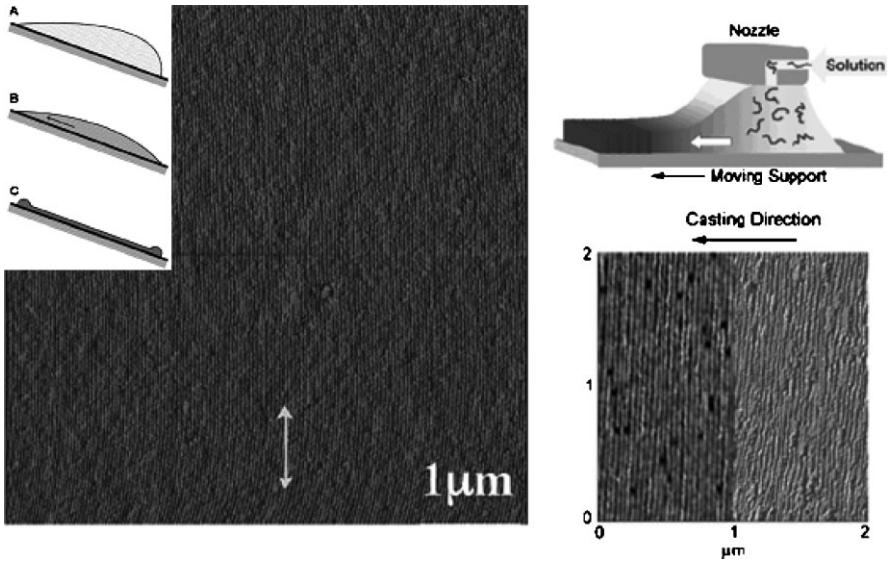

Figure 7. Left: AFM image of the oriented PS-*b*-PB feature by directional evaporation; Insert: schematic diagrams of a block copolymer solution droplet drying on a tilted substrate where the solution is pinned to the substrate. A directional convection (arrow direction) is in the droplet during evaporation.[60] Copyright 2003 American Chemical Society. Reproduced with permission. Right: Schematic diagrams and AFM images of long-range order in thin films of PBA-*b*-PAN block copolymers prepared by zone-casting.[61] Copyright 2005 American Chemical Society. Reproduced with permission.

on the substrate, and, ii) use of EUV-IL to form the chemical pattern (Figure 8, left). When the periodicity of the chemical patterns on the substrate matched that of the lamellar microdomains of the BCPs, the microphase separation feature was highly oriented and defect-free. This method can provide precise control of microdomains on surfaces even for complex pattern geometries containing bends, T-junctions and jogs (Figure 8, top right). A technique recently developed by Cheng et al.[66] in preparing complex patterns is considered to be one of the most hopeful methods in preparing defect-free nanofeatures. They used sparse chemical patterns to achieve defect-free alignment of PS-*b*-PMMA lamellae, from which it was possible to double, triple and quadruple the frequencies of surface chemical patterns using BCPs. Since the methods could afford frequency multiplication and supply sharp chemical contrast in the nanoscale features of the BCP's self-assembly, directed self-assembly was brought one step closer to practical application (Figure 8, bottom right). However, chemical patterns guiding is same as for graphoepitaxy, which still depends on photolithography.

Orientation of Microphase Separation Induced by an External Field

Shear

In BCP thin films, a preferential orientation direction of the nanostructure can spontaneously form below the T_d. Without any boundary confinements or external field guide, this spontaneous orientation is undetermined and occurs randomly – since the system is isotropic – from which BCPs tend to phase separate into a microscale multigrain structure with a nanoscale periodicity. Although such a multigrain structure has isotropic properties macroscopically, this feature is still far away from application because of the low order at the microscale. However, by using shear to break the system isotropic property, BCPs can phase separate in orientation, which exhibits a surprising variety of phase separation features in the BCP bulk[67,68] (Figure 9, left). Furthermore, the microdomains of the BCP thin films can also be oriented by shearing. For example, Angelescu et al.[69] aligned cylindrical PS microdomains in a PS-*b*-poly(ethylene-*alt*-propylene) (PS-*b*-PEP) di-BCP thin film under the shear of a poly(dimethylsiloxane) (PDMS) pad at 100 °C, where the film thickness was 50 nm. Figure 9 (right) shows atomic force microscopy (AFM) images of the BCP microdomains aligned by shearing. Besides orienting microdomains of the BCP thin films, strong shear can also induce a phase transition in the BCP microdomains. Hong et al.[70] recently applied strong shear to sphere-forming PS-*b*-PI thin films, and found that the strong shear could both generate orientational order and induce a feature transition from the spherical phase to the cylindrical phase at high stress. In their experiments, they also found that, the more asymmetric di-BCP was sheared, the higher stress was required for the phase transition. When the stress was below the critical value of the phase transition, the shear simply distorted the hexagonal lattice formed by the spherical

Macromol. Rapid Commun. **2010**, *31*, 591–608

Macromolecular Journals
DOI: 10.1002/marc.200900541

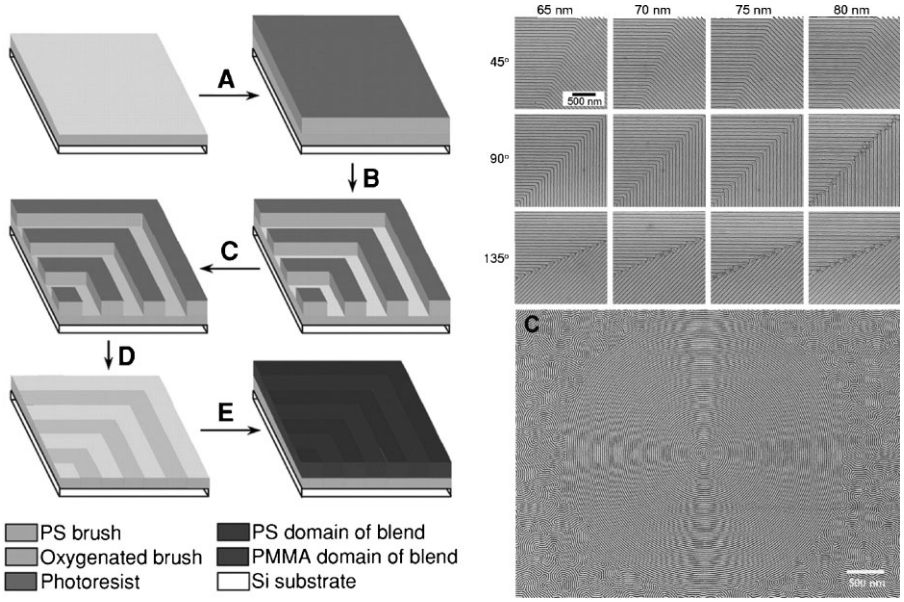

Figure 8. Left: Schematic of the use of chemically nanopatterned surfaces to direct the self-assembly of ternary blends in linear and bend geometries.[65] Copyright 2005 American Association for the Advancement of Science. Reproduced with permission. Top right: SEM images of angled lamellae in a ternary PS-*b*-PMMA/PS/PMMA blend.[65] Copyright 2005 American Association for the Advancement of Science. Reproduced with permission. Bottom right: SEM micrograph of self-assembly feature by chemical guiding patterns.[66] Copyright 2008 Wiley-VCH Verlag GmbH & Co. KGaA. Reproduced with permission.

phase. Recently, Jung et al.[71] also found that shear could also induce crystallization and orient crystals in semi-crystalline and ferroelectric BCPs. In their experiments, they employed a static shear to control both molecular and microstructural orientation of semi-crystalline and ferroelectric poly(vinylidene fluoride-*co*-trifluoroethylene) (PVDF-TrFE) thin films. They found a sheared film exhibited a monolithic single-crystal-like texture, and the approximately 25 nm thick crystalline lamellae were oriented almost perpendicular to the shear direction in the film. In summary, shear is a simple and efficient method to orient the microdomains of the BCP thin films; however, the low uniformity of the shearing force is the bottleneck to achieve long-range high-ordered microdomains.

Electric Field

In contrast to the temperature gradient and shearing force, the electric field is a simple and more controllable external field, which can also be used to orient the microdomains of BCPs.[72] Russell et al. found that BCPs with high contrast in

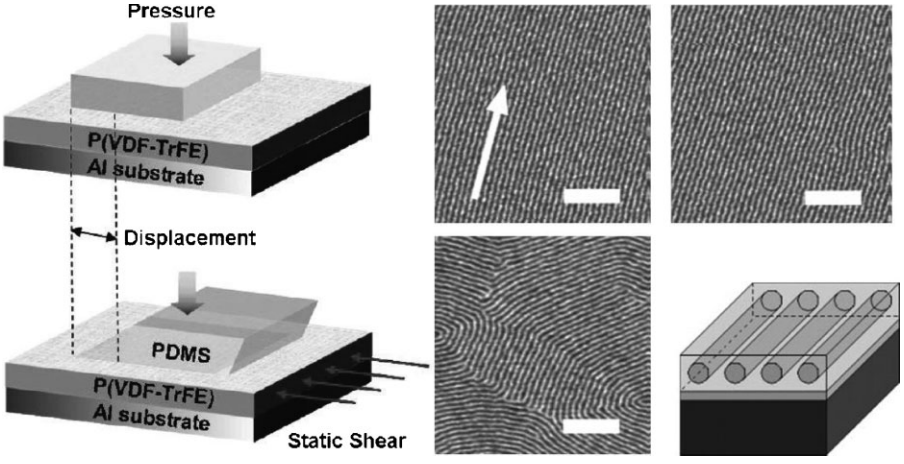

Figure 9. Left: Schematics of static shearing a polymer thin film by a PDMS pad.[71] Copyright 2009 American Chemical Society. Reproduced with permission. Right: AFM images of a PS-*b*-PI copolymer sample aligned by shearing with a PDMS pad. The arrow indicates the shearing direction. Scale bar represents 250 nm.[69] Copyright 2004 Wiley-VCH Verlag GmbH & Co. KGaA. Reproduced with permission.

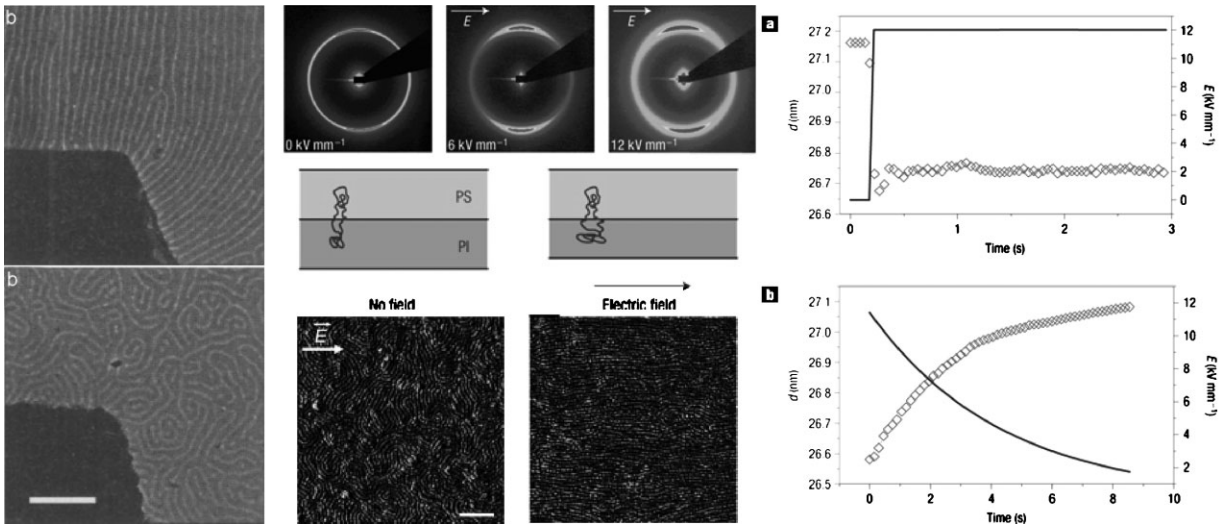

Figure 10. Left: TEM images of a PS–PMMA cylinder phase near an electrode in the presence of an applied electric filed (top, 37 kV · cm^{-1}) and in the absence of an applied electric field (bottom). The scale bar represents 500 nm.[73] Copyright 1996 American Association for the Advancement of Science. Reproduced with permission. Middle top: Reversible lamellar structure of PS-*b*-PI controlled by an electric field.[74] Copyright 2007 Nature. Reproduced with permission. Middle bottom: Orientational order in a block copolymer via a gradient electric field.[75] Copyright 2008 American Chemical Society. Reproduced with permission. Right: Time dependence of the lamellar distance of aligned lamellae with increasing (top) and decreasing (bottom) electric-field strength.[74] Copyright 2007 Nature. Reproduced with permission.

dielectric permittivity between the two blocks could be aligned (when the polymer is fluid) in a large electric field (typically tens or hundreds of kV · cm^{-1}).[73] Figure 10 (left) shows the alignment of PMMA cylinders in PS-PMMA along electric field lines radiating in-plane from an electrode, contrasted to the case where no electric field was applied. This technique supplies an easy pathway to orient the microdomains of BCPs. Schmidt et al.[74] took advantage of electric fields to reversibly tune the nanolamellar structure of PS-*b*-PI di-BCP with high accuracy (as much as 6% in a completely reversible way on a timescale of the order of several milliseconds) (Figure 10, top middle). They found that the lamellar distance decreased as the chain conformation entropy increased when the lamellar structure was aligned parallel to the field direction because the electric field counteracted the stretching induced by the microphase separation. On the other hand, the lamellar spacing increased and the conformational entropy decreased when the lamellae were oriented perpendicular to the electric-field direction. The switching time of the process is considerably smaller than 45 ms (Figure 10, right). Since the gradient electric field can be employed to investigate the minimum field strength at which the microdomains orient in the applied field; recently, Olszowka et al.[75] demonstrated a combinatorial approach. They used a gradient electric field in one experiment to investigate how strong an electric field should be used to align a given BCP system. They also found[75] that, by increasing the dielectric contrast of the polymer blocks, a reduced threshold field strength and an improved orientation of the lamellae could be achieved (Figure 10, bottom middle).

Magnetic Field

We have summarized that applying an external electric field is a simple and controllable way to induce the orientation of the micro-domains in the BCP thin films. However, a crucial problem – the dielectric breakdown problem – cannot be avoided in this method, which distinctly limits the applicability of the electric field for orienting the microdomains of a BCP film, and causes a limitation to the maximal field power. However, besides electric fields, similar effects are anticipated for magnetic fields. In an electric field, the spatial modulation of the dielectric constant determines the free energy of the system, while the magnetic permeability determines the free energy in case of using a magnetic field. Without dielectric breakdown concern, the magnetic field has superiority in application – the film thickness must not necessarily be thin.[76] Sakurai et al.[76] conducted thermal annealing in the presence of a 30 T magnetic field to polystyrene-*block*-poly(ethylene-butylene)-*block*-polystyrene (SEBS) thin films with thickness ranging from 20 to 300 nm. Cylindrical microdomains were obtained for the freely-annealed sample without any preferential orientation, as observed in Figure 11. However, with thermal annealing (at 180 °C for 3–5 h) in the presence of the magnetic field, the film re-self-assembled, and the cylindrical microdomains

Macromol. Rapid Commun. **2010**, *31*, 591–608

Macromolecular Journals
DOI: 10.1002/marc.200900541

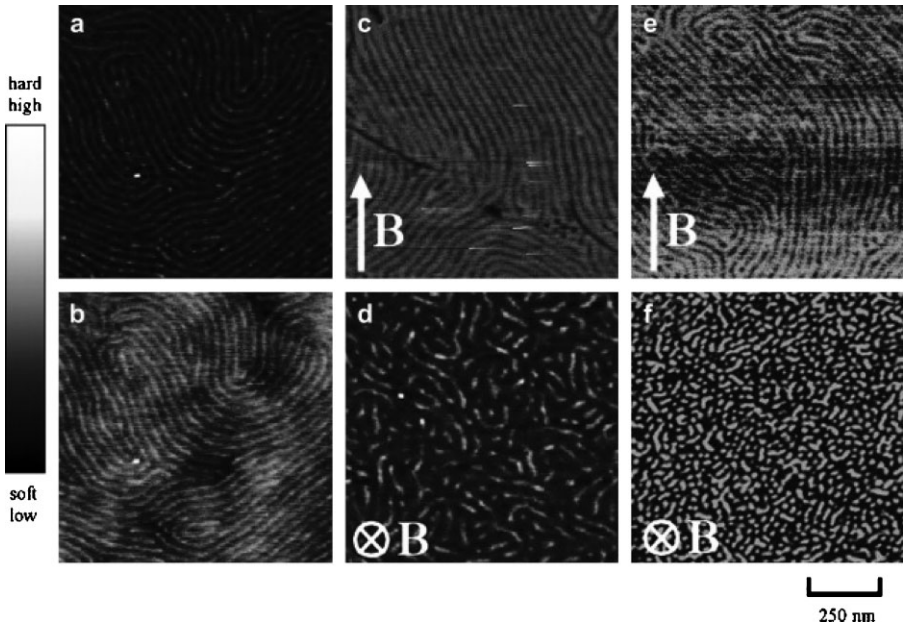

Figure 11. AFM images of a 20 nm thick film annealed at 180 °C for 12 h in the absence of the 30 T magnetic field: a) phase image, b) corresponding height image, c) 20 nm thick film, annealed for 3 h in horizontal magnetic field, d) 20 nm thick film, annealed for 3 h in vertical magnetic field, e) 60 nm thick film, annealed for 5 h in horizontal magnetic field, and, f) 300 nm thick film, annealed for 5 h in vertical magnetic field.[76] Copyright 2008 Elsevier. Reproduced with permission.

were oriented according to the magnetic field direction. They also found that the orientation degree distinctly depended on the comparability between film thickness and the diameter of the cylinder diameter (13 nm). Moreover, a preferential orientation of the cylinders parallel to the direction of the applied magnetic field was also found when the magnetic field was parallel to the substrate (Figure 11c). However, the panel does not contain a patch of the homeotropic orientation of cylinders, although a reorienting cylinder was detected by a perpendicular magnetic field (Figure 11d). The authors believed the film thickness to be too thin to overcome the surface affirmative interaction due to a spatial confinement in thin films (the film thickness could induce physical constraints on the formation and the orientation of the microdomains).[76]

Evolution, Order–Order Transition and Reversible Switching of Microdomains by Solvent-Vapor-Annealing

Thanks to the rapid growth in smart device applications over recent decades, various efforts have been made towards the development of intelligent surfaces, on which surface features, such as wettability or adhesion, are controllable and responsive to environmental conditions, such as pH, temperature, light and the presence of a specific chemical substrate. Herein, we will summarize progress towards fabricating intelligent BCP films, on which microdomains can continuously evolve, transit, or reversibly switch among ordered features by solvent-vapor-annealing.

Evolution of the Microdomains by Solvent-Vapor-Annealing

During the solvent-vapor-annealing process, many well-ordered metastable microphase separation features can be observed and the microdomains evolve continuously with the annealing time (t),[77–79], since the degree of diffusion of the solvents in the film and the movements of polymer molecules are time-dependent. For example, when two PS-*b*-PMMA thin films pf the same composition were annealed in acetone vapor at different pressures, two series of microdomains were observed, clearly functions of the annealing time (t).[77] In a high or low vapor pressure, both nanoporous and nanoprotuberant structures disappeared, and a series of different microdomains formed depending on the annealing time, including well-ordered hexagonally-packed nanocylinders, highly ordered nanoscopic spheres or stripes, and a novel so-called flower-like pattern, which was comprised of six PS spheres, each sphere belonging to three "flowers". Finally, both films showed stripe features but of different sizes (Figure 12, top).[78] This feature evolution is due to the high attraction between acetone and the PMMA block. In acetone vapor, the enriched PMMA phase on the substrate tends to move to the film surface. The

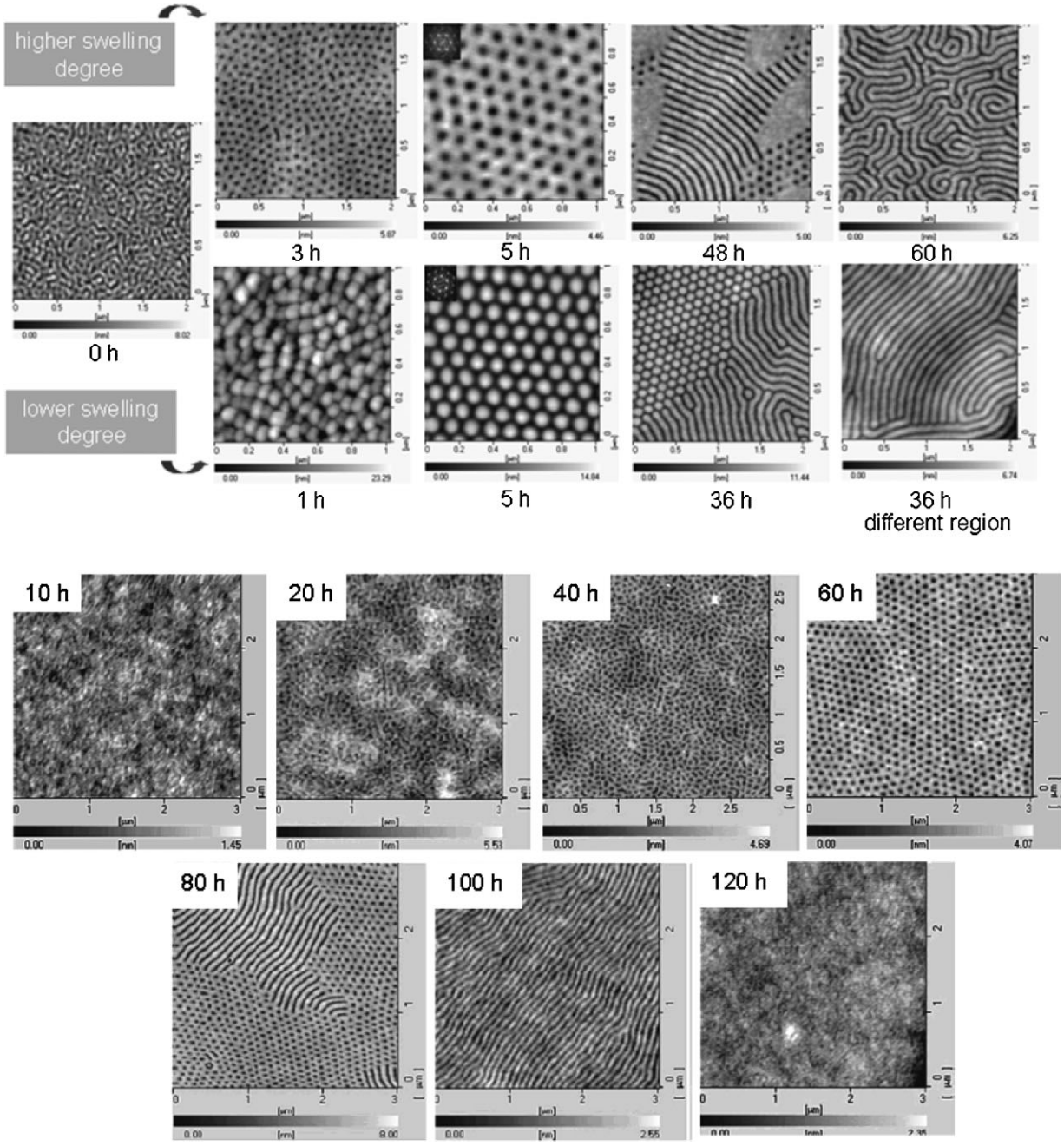

Figure 12. Feature evolution of PS-*b*-PMMA microphase separation in solvent vapor annealing with various annealing time. Top: AFM images of symmetrical PS-*b*-PMMA film morphology evolution under high and low acetone vapor pressure.[77,78] Copyright 2005 Wiley-VCH Verlag GmbH & Co. KGaA. Reproduced with permission. Bottom: AFM images of symmetrical PS-*b*-PMMA film morphology evolution under chloroform vapor.[79] Copyright 2004 American Chemical Society. Reproduced with permission.

amount of PMMA phase on the surface increased and connected gradually to form stripes.

Similar feature evolution was also observed when the thin PS-*b*-PMMA film was annealed in chloroform vapor, a selective solvent to the PMMA block, where the film thickness was less than L_0.[79] With increasing annealing time in a saturated chloroform vapor, a series of microphase separation features developed from a disordered microstructure, to well-ordered hexagonally-packed nanocylinders, to a mixed morphology containing nanocylinders and stripes, to stripes and, finally, switching back to the flat surface (Figure 12, bottom). It is reasonable to consider that, after being spin-coated onto the wafer substrate, the PMMA block dominated the substrate and the PS block formed a

Macromol. Rapid Commun. **2010**, *31*, 591–608

DOI: 10.1002/marc.200900541

continuous layer at the film–air interface. Since the PMMA block is more soluble in chloroform, there is a strong attractive interaction between the polymer and the solvent, and the net interaction between the polymer segments is repulsive. As the result, the coiled chains started to swell as soon as they came into contact with the solvent molecules. Elevated solvent treatment time increased the diffusivity of the polymer component in the thin film. Given enough annealing time under conditions of relatively high diffusivity, the films would adopt their thermodynamically stable states. Shorter annealing times effectively freeze in some metastable features. With increasing treatment time, more and more PMMA segments occupied the film surface. Therefore, well-ordered hexagonally-packed nanocylinders could be obtained at a certain annealing time.

In summary, the solvent annealing time is a key factor for the evolution of microphase-separated morphology, which can be changed from a disordered state to a nanoscale depression morphology and, finally, to strips.

The film thickness can also govern the microdomain evolution in solvent-vapor-annealing. For example, when a symmetric PS-*b*-PMMA thin film is annealed in chloroform or acetone vapors (selective solvents to the PMMA block), well-ordered hexagonally-packed nanocylinders can form by microphase separation. However, this feature is strictly confined by the film thickness.[79] Figure 13 shows the microdomain evolution of symmetric PS-*b*-PMMA thin films in response to the different film thickness when the films were exposed in chloroform vapor for 60 h, where the film thickness was controlled by spin-coating BCP solutions having different concentrations (at the same spin-coating speed, concentrations of 0.4, 0.6, 0.8 and 1 wt.-% correspond to film thicknesses of 19, 26, 38 and 54 nm, respectively.). Well-ordered hexagonally-packed nanocylinders were obtained when the film thicknesses was 19, 26 and 38 nm, less than $1/2L_0$. In a PMMA-selective solvent vapor, the PMMA block has a high mobility, and can reconstruct itself easily. Surface-perpendicular PMMA protrusions of approximately $L_0/2$ in width perforate the PS layer in response to the chloroform or acetone attraction. When the film thickness is less than $1/2L_0$, well-ordered hexagonally packed nanocylinders tend to minimize the total energy. Otherwise, when the film thickness is larger than $1/2L_0$, the film has a thicker PS layer at the top; the elongated stripe domains that are so-called perpendicular lamella are perpendicular to the substrate. In summary, if the BCP film thickness is less than the threshold film thickness T ($1/2L_0$ is around 45 nm in ref. [64]), the films exhibit surface-parallel or surface-perpendicular morphology. Otherwise, the films exhibit the unconventional morphology of well-ordered hexagonally packed cylinders.

Order–Order Transition in Tri-Block Copolymer (Tri-BCP) Thin Films

In contrast to di-BCPs, tri-BCPs can show much more complicated and richer microphase separation features during annealing in solvent vapors.[80,81] Therefore, the order–order transition (OOT) of tri-BCP thin film is certainly of interest especially when undergoing the transition from the gyroid (G) phase to the other adjacent phases because of the potential application in designing smart features. However, the phase-to-phase transitions have been little studied since Krausch et al.[82] observed the co-existence of gyroid (112) [G (112)] and cylinder (001) [C (001)] in PS-*block*-poly(2-vinylpyridine)-*block*-poly(tert-butyl methacrylate) (SBV) tri-BCP thin film annealed in chloroform vapor. Due to the solvent vapors used to induce the OOT process in the thin SBV tri-BCP film not being neutral, we believed until recently that the observed OOT processes – in the sequence cylinder (C) ↔ sphere in 'diblock gyroid' (sdG) ↔ sphere in lamella (sL) ↔ sphere (S) – were driven by the different affinity among the solvent molecules and the three compositions. The epitaxial OOT process in the sequence of C (001) ↔ G (111) ↔ dG (211) ↔ sdG $(110)_{0.25}$ ↔ sdG $(110)_{0.1875}$ ↔ sL (001) ↔ S in thin SBV tri-BCP film has been induced in a saturated benzene vapor at room temperature (Figure 14),[83] which was driven by the different affinity between the solvent molecules and the three blocks. We found sdG (111) could epitaxially grow from C (001) on the film surface, while the lamella formed from gyroid with

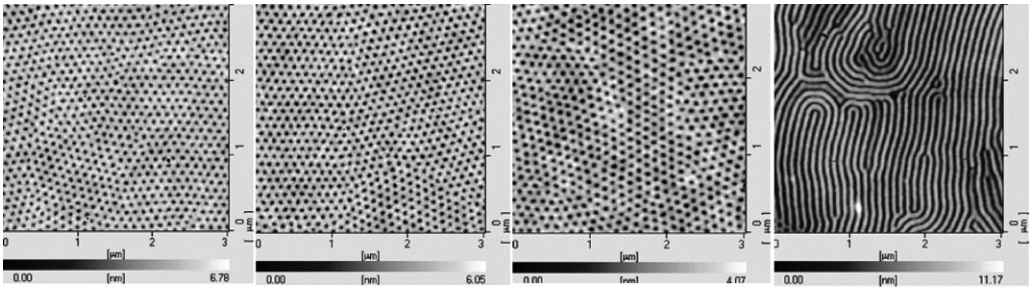

Figure 13. AFM images of symmetrical PS-*b*-PMMA films with different film thickness annealing in chloroform vapor for 60 h.[79] Copyright 2004 American Chemical Society. Reproduced with permission.

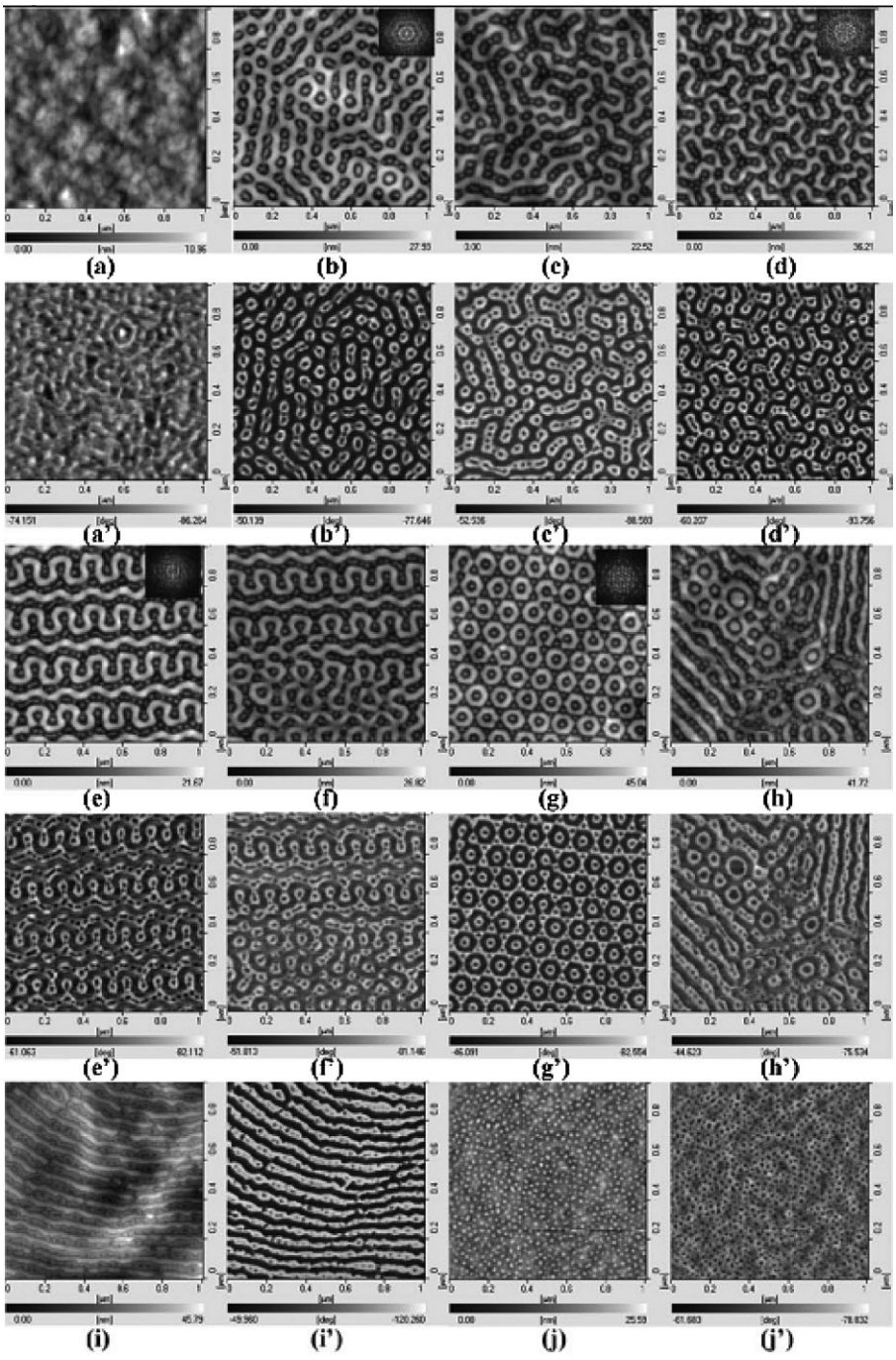

Figure 14. AFM images of the surface morphology evolution of the thin SBV film on the silicon substrate treated in benzene vapor at room temperature for different time: a) 0, b) 3, c) 18, d) 24, e) 48, f) 58, g) 72, h) 100, i) 132, j) 168 h. a'–j' are the corresponding phase images of a–j, respectively. The insets in b, d, e, g are the 2D-Fourier transform patterns of the corresponding AFM topography images, respectively.[83]

the epitaxial relation of sdG $(110)_{0.1875} \leftrightarrow$ sL (001) due to their total surface areas being nearly equal to each other. Finally, only the P2VP spheres remained in the film because the S and B blocks became compatible with the decrease of the copolymer concentration.

Among C, sdG, and sL phases, PB has the smallest surface area in C phase and the largest surface area in L phase, where the surface areas of P2VP are almost fixed. We believe this is due to the preferential contact between benzene molecules and the PS blocks, which tended to

Macromol. Rapid Commun. **2010**, *31*, 591–608

Macromolecular Journals
DOI: 10.1002/marc.200900541

separate PS and the other two blocks. Therefore, the interface area between PS and the other two blocks decreases via annealing the film in benzene vapor. Accordingly, C phase forms the smallest surface area of the PB blocks initially. Furthermore, with the increasing diffusion of solvent molecules, the sdG phase gradually emerges on the surface because the interface between PS and PB blocks weakens under the interaction between the solvent and the PB phase.

The epitaxial phase transition [C (001) ↔ sdG (111)] is due to the formation of one fivefold junction that pinches off, breaking a cylinder and leaving a threefold junction. Given the increasing interaction between benzene molecules and the PB phase, the effective fraction of PB molecules improves distinctly. The packing chains generate an unstable void in the middle of the PB domains. To avoid unstable void formation, PB chains stretch to fill the space, and sphere in lamella (sL) phase forms. Since the interaction between the top surface of the SBV film and the surrounding solvent vapor was much stronger than that between the SBV film and the underlying substrate (silicon, mica or carbon-coated mica), the transition from gyroid symmetry to lamella was more dependent on the benzene vapor. However, when the film was annealed in a saturated CS_2 vapor, a strong selective solvent to PS and P2VP blocks, the different OOT process with, specifically hexagonally-arranged core–shell cylinder and double-hexagonally-arranged-dots, could be observed when the film thickness was around 44, 123 and 223 nm. When the film thickness was decreased to 13 nm, the ordered structure was absent in the SBV thin film.[84] Moreover, the controllable OOT process of SBV thin film could be induced in solvents by blending SBV with homo-PS.[85] When the fraction of homo-PS was less than 10 wt.-%, the OOT sequence 'C → sdG → sL → S' was observed, whereas PS domain area at the surface improved. However, when the fraction of homo-PS was in the range 10–30 wt.-%, this was replaced by a different OOT process: 'hexagonally-arranged core–shell cylinder' to 'sphere in lamella → double spheres'. In summary, in contrast to the pure SBV thin films annealed in benzene vapors, the blending thin films have totally different phase behaviors, which are strictly governed by the added home-PS fraction, that is, the effective volume fraction of the PS phase.

Reversible Switching Microdomains by Solvent-Vapor-Annealing

Reversible switching surfaces have also attracted great interest. In these, the surface morphology or composition is reversibly stimuli-responsive to the environmental variations. Recently, Peng et al.[86] found reversible switching microdomains could be achieved by annealing BCP thin films in solvent vapors. The microdomains of a PS-*b*-PMMA thin film exhibited surface reorganization in response to selective solvent annealing (Figure 15).[86] After annealing in acetone vapor at high pressure for 5 h, the PS-*b*-PMMA thin film can phase-separate into a well-ordered hexagonally-packed nanoporous structure. However, after exposing the treated film to CS_2 vapor – a selective solvent to the PS block but a poor solvent to the PMMA block – for 80 min, the nanoporous microdomains changed to an ordered hexagonally-packed nanoprotuberant structure.

Figure 15 shows the reversible switching of microdomains on annealing PS-*b*-PMMA film in different selective solvent vapors. This morphology switching is caused by the different behaviors of the PS and PMMA chains in their selective solvent vapors. Upon annealing in acetone vapor for different times, both PS and PMMA blocks are present at the depressions or striped film surface. After annealing in CS_2 vapor, the PMMA block migrates to the film/solvent interface, and forms aggregates with neighboring PMMA block to avoid contact with the solvent. On the other hand, the PS block is swollen by CS_2 and migrates to the film/solvent interface to form a shield around the PMMA aggregates. Both effects lead to an opposite movement between the two blocks, and the top part of the film will be dominated by PS chains and turn hydrophobic. Thus, eventually an ordered hexagonally-packed nanoprotuberant feature forms in the film. However, after annealing the film again in acetone vapor, the morphology reversibly switches back to the original state. It was found the evolution time of the switching process from the nanopor-

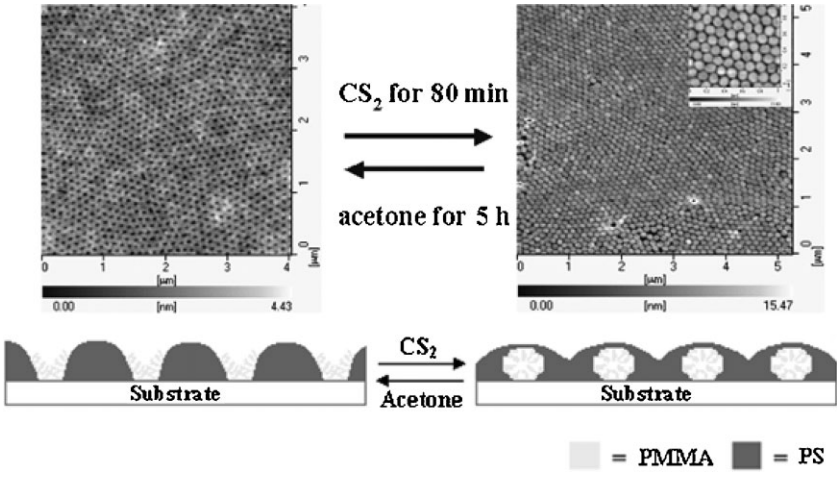

Figure 15. AFM and schematic images of symmetrical PS-*b*-PMMA film morphology switching in acetone and CS_2 vapors.[86] Copyright 2004 American Institute of Physics. Reproduced with permission.

ous feature to the nanoprotuberant one was faster than that of the reverse process.

The different evolution time is believed to occur for the following reason: in CS_2 vapor, both components are present at the surface, and CS_2 vapor penetrates and swells the PS domains; however, in acetone vapor, there is no direct contact between the lower PMMA aggregates and the acetone vapor, so the solvent molecules must diffuse through the upper PS domains to reach the interior PMMA aggregates, which delays the evolution process. Having such a sensitive reversible switching-property in morphology and wettability, the BCP film is an excellent candidate for fabricating smart surfaces and designing chemical sensors.

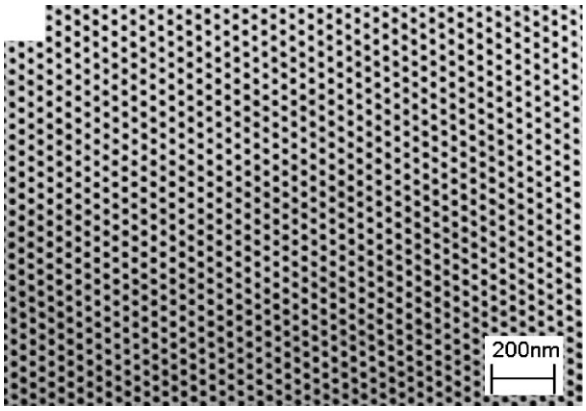

Figure 16. SEM image of relative long-range ordered arrays from microphase separation of PS-*b*-PMMA thin film.[87] Copyright 2009 American Chemical Society. Reproduced with permission.

Conclusion

Today, micro/nano-patterned surfaces are widely used in many areas, such as in preparation of super-thin dielectric films, photonic crystals, antireflective films, super-non-wetting surfaces, bio-compatible surfaces, etc. Developing micro/nano-patterning techniques is a promising subject in surface science. Since photolithography can supply high resolution and long-range ordered features, it has been widely used in the fabrication of electric devices. However, the irreducible high cost and the rigorous fabrication conditions required are leading to rapid growth in alternative techniques, especially in pattering nano-scale devices. Therefore, BCP microphase separation, which can supply 10–50 nm patterns, has been identified as a way to pattern nanostructured polymer surfaces. Meanwhile, the patterned surfaces can also be used as a pre-patterned template for lithography.

In contrast to traditional lithography, microphase separation of BCP thin films is lower cost, easier with respect to fabrication, and can achieve complex, special surface compositions and nanoscale patterns. However, achieving long-range ordered arrays is the main challenge for this technique. As discussed in this paper, although chemical guiding patterns can now achieve some long-range ordered arrays, the pre-patterned substrates also depend on the lithography technique.[64–66] Therefore, several other techniques have been developed, but these are still immature as illustrated by the breakdown problem in electric field induced methods, low uniformity of the temperature gradient, shear force, etc. Recently, Han et al.[87] achieved a relative long-range ordered array by critically controlling the fraction of each block, the annealing temperature, the film thickness and the substrate (Figure 16), which is a great beginning from which to achieve long-range ordered arrays. Moreover, polymer films with switchable surface compositions or morphologies have been considered for use as smart surfaces, which can be widely used to fabricate intelligent optical/electric/bio-chips and devices. In conclusion, stimuli-responsive microphase separation in BCP thin films is also an efficient technique in patterning smart features.

Acknowledgements: This work was financially supported by the *National Natural Science Foundation of China* (20621401, 20834005), the *Chinese Academy of Sciences* (KJCX2-YW-M11) and the *Ministry of Science and Technology of China* (2009CB930603).

Received: August 1, 2009; Revised: October 23, 2009; Published online: January 18, 2010; DOI: 10.1002/marc.200900541

Keywords: block copolymers; lithography; microphase separation; nanoheterogeneity

[1] Y. Xia, G. M. Whitesides, *Angew. Chem., Int. Ed.* **1998**, *37*, 550.
[2] K. S. Park, E. K. Seo, Y. R. Do, K. Kim, M. M. Sung, *J. Am. Chem. Soc.* **2006**, *128*, 858.
[3] http://www.semiconductor.net/article/CA6622435.html.
[4] http://www.semiconductor.net/article/206026-Lithography_for_the_22_nm_Node.php.
[5] [5a]"*Developments in Block Copolymer Science and Technology*", I. W. Hamley, Ed., John Wiley and Sons, 2004; [5b] J. Bang, U. Jeong, D. Yeol, T. P. Russell, C. J. Hawker, *Adv. Mater.* **2009**, *21*, 1.
[6] D. Beattie, K. H. Wong, C. Williams, L. A. Poole-Warren, T. P. Davis, C. Barner-Kowollik, M. H. Stenzel, *Biomacromolecules* **2006**, *7*, 1072.
[7] M. M. de Villiers, P. Aramwit, G. S. Kwon, "*Nanotechnology in Drug Delivery*", Springer, New York 2009.
[8] E. V. Rogozhina, J. Werner, H. Kresse, S. A. Kuptsov, R. V. Talroze, *Macromolecules* **1999**, *32*, 3379.
[9] [9a] P. J. Flory, *J. Chem. Phys.* **1941**, *9*, 660; [9b] M. L. Huggins, *J. Chem. Phys.* **1941**, *9*, 440.

Macromol. Rapid Commun. **2010**, *31*, 591–608

DOI: 10.1002/marc.200900541

[10] F. S. Bates, G. H. Fredrickson, *Annu. Rev. Phys. Chem.* **1990**, *41*, 525.
[11] L. Leibler, *Macromolecules* **1980**, *13*, 1602.
[12] A. Alexander-Katz, G. H. Fredrickson, *Macromolecules* **2007**, *40*, 4075.
[13] K. Almdal, J. H. Rosedale, F. S. Bates, G. D. Wignall, G. H. Fredrickson, *Phys. Rev. Lett.* **1990**, *65*, 1112.
[14] F. S. Bates, G. H. Fredrickson, *Phys. Today* **1999**, *52*, 32.
[15] M. M. Mok, S. Pujari, W. R. Burghardt, C. M. Dettmer, S. T. Nguyen, C. J. Ellison, J. M. Torkelson, *Macromolecules* **2008**, *41*, 5818.
[16] K. Karaky, L. Billon, C. Pouchan, J. Desbrières, *Macromolecules* **2007**, *40*, 458.
[17] M. J. Fasolka, A. M. Mayes, *Annu. Rev. Mater. Res.* **2001**, *31*, 323.
[18] R. Limary, P. F. Green, *Macromolecules* **1999**, *32*, 8167.
[19] L. Leibler, *Macromolecules* **1980**, *13*, 1602.
[20] A. Alexander-Katz, G. H. Fredrickson, *Macromolecules* **2007**, *40*, 4075.
[21] A. P. Smith, J. F. Douglas, E. J. Amis, A. Karim, *Langmuir* **2007**, *23*, 12380.
[22] T. Hashimoto, J. Bodycomb, Y. Funaki, K. Kimishima, *Macromolecules* **1999**, *32*, 952.
[23] J. Bodycomb, Y. Funaki, K. Kimishima, T. Hashimoto, *Macromolecules* **1999**, *32*, 2075.
[24] B. C. Berry, A. W. Bosse, J. F. Douglas, R. L. Jones, A. Karim, *Nano Lett.* **2007**, *7*, 2789.
[25] K. Mita, H. Tanaka, K. Saijo, M. Takenaka, T. Hashimoto, *Macromolecules* **2007**, *40*, 5923.
[26] K. Mita, H. Tanaka, K. Saijo, M. Takenaka, T. Hashimoto, *Macromolecules* **2008**, *41*, 6787.
[27] K. Fukunaga, H. Elbs, R. Magerle, G. Krausch, *Macromolecules* **2000**, *33*, 947.
[28] K. Fukunaga, T. Hashimoto, H. Elbs, G. Krausch, *Macromolecules* **2002**, *35*, 4406.
[29] H. Elbs, K. Fukunaga, R. Stadler, G. Sauer, R. Magerle, G. Krausch, *Macromolecules* **1999**, *32*, 1204.
[30] S. Walheim, M. Böltau, J. Mlynek, G. Krausch, U. Steiner, *Macromolecules* **1997**, *30*, 4995.
[31] H. Elbs, C. Drummer, V. Abetz, G. Krausch, *Macromolecules* **2002**, *35*, 5570.
[32] S. Niu, R. F. Saraf, *Macromolecules* **2003**, *36*, 2428.
[33] Y. Chen, H. Huang, Z. Hu, T. He, *Langmuir* **2004**, *20*, 3805.
[34] G. Kim, M. Libera, *Macromolecules* **1998**, *31*, 2569.
[35] G. Kim, M. Libera, *Macromolecules* **1998**, *31*, 2670.
[36] S. H. Kim, M. J. Misner, T. Xu, M. Kimura, T. P. Russell, *Adv. Mater.* **2004**, *16*, 226.
[37] J. Peng, D. H. Kim, W. Knoll, Y. Xuan, B. Li, Y. Han, *J. Chem. Phys.* **2006**, *125*, 064702.
[38] [38a] C. Park, J. Yoon, E. L. Thomas, *Polymer* **2003**, *44*, 6725; [38b] J. Bang, U. Jeong, D. Y. Ryu, T. P. Russell, C. J. Hawker, *Adv. Mater.* **2009**, *21*, 1.
[39] I. W. Hamley, J. P. A. Fairclough, N. J. Terril, A. J. Ryan, P. M. Lipic, F. S. Bates, E. Town-Andrews, *Macromolecules* **1996**, *29*, 8835.
[40] J. P. A. Fairclough, S. M. Mai, W. Bras, L. Messe, S. C. Turner, A. J. Gleeson, C. Booth, I. W. Hamley, A. J. Ryan, *J. Chem. Phys.* **2001**, *114*, 5425.
[41] L. Zhu, S. Z. D. Cheng, B. H. Calhoun, Q. Ge, R. P. Quirk, E. L. Thomas, B. S. Hsiao, F. Yeh, *J. Am. Chem. Soc.* **2000**, *122*, 5957.
[42] P. Huang, L. Zhu, S. Z. D. Cheng, Q. Ge, R. P. Quirk, E. L. Thomas, B. Lotz, B. S. Hsiao, F. Yeh, *Macromolecules* **2001**, *34*, 6649.
[43] L. Zhu, P. Huang, S. Z. D. Cheng, Q. Ge, R. P. Quirk, E. L. Thomas, B. Lotz, J. C. Wittmann, B. S. Hsiao, F. Yeh, L. Liu, *Phys. Rev. Lett.* **2001**, *86*, 6030.
[44] L. Zhu, P. Huang, W. Y. Chen, Q. Ge, R. P. Quirk, S. Z. D. Cheng, E. L. Thomas, B. Lotz, B. S. Hsiao, F. Yeh, L. Liu, *Macromolecules* **2002**, *35*, 3553.
[45] L. Zhu, S. Z. D. Cheng, P. Huang, Q. Ge, R. P. Quirk, E. L. Thomas, B. Lotz, B. S. Hsiao, F. Yeh, L. Liu, *Adv. Mater.* **2002**, *14*, 31.
[46] I. W. Hamley, E. L. Hiscutt, Y. W. Yang, C. Booth, *J. Colloid Interface Sci.* **1999**, *209*, 255.
[47] G. Reiter, G. Castelein, P. Hoerner, G. Riess, A. Blumen, J. Sommer, *Phys. Rev. Lett.* **1999**, *83*, 3844.
[48] L. Royer, *Bull. Soc. Fr. Mineral Crystallogr.* **1928**, *51*, 7.
[49] J. H. van deer Mere, *Faraday Discuss.* **1949**, *5*, 206.
[50] G. S. Swei, J. B. Lando, S. E. Rickert, K. A. Mauritz, *Encycl. Polym. Sci. Eng.* **1986**, *6*, 209.
[51] C. De Rosa, C. Park, B. Lotz, L. J. Fetters, J. C. Wittmann, E. L. Thomas, *Macromolecules* **2000**, *33*, 4871.
[52] [52a] R. A. Segalman, H. Yokoyama, E. J. Kramer, *Adv. Mater.* **2001**, *13*, 1152; [52b] R. A. Segalman, A. Hexemer, E. J. Kramer, *Phys. Rev. Lett.* **2003**, *91*, 196101/1; [52c] R. A. Segalman, A. Hexemer, E. J. Kramer, *Macromolecules* **2003**, *36*, 6831; [52d] R. A. Segalman, K. E. Schaefer, G. H. Fredrickson, E. J. Kramer, S. Magonov, *Macromolecules* **2003**, *36*, 4498.
[53] S. M. Park, M. P. Stoykovich, R. Ruiz, Y. Zhang, C. T. Black, P. F. Nealey, *Adv. Mater.* **2007**, *19*, 607.
[54] J. Y. Cheng, J. Pitera, O. H. Park, M. Flickner, R. Ruiz, C. T. Black, H. C. Kim, *Appl. Phys. Lett.* **2007**, *91*, 143106.
[55] S. M. Park, C. T. Rettner, J. W. Pitera, H. C. Kim, unpublished.
[56] H. C. Kim, C. T. Rettner, L. Sundstrom, *Nanotechnology* **2008**, *19*, 235301.
[57] S. J. Jeong, J. E. Kim, H. S. Moon, B. H. Kim, S. M. Kim, J. B. Kim, S. O. Kim, *Nano Lett.* **2009**, *6*, 2300.
[58] E. Bodenschatz, W. Pesch, G. Ahlers, *Annu. Rev. Fluid. Mech.* **2000**, *32*, 709.
[59] S. J. Vanhook, M. F. Schatz, J. B. Swift, W. D. McCormick, *J. Fluid Mech.* **1997**, *345*, 45.
[60] M. Kimura, M. J. Misner, T. Xu, S. H. Kim, T. P. Russell, *Langmuir* **2003**, *19*, 9910.
[61] C. Tang, A. Tracz, M. Kruk, R. Zhang, D. M. Smilgies, K. Matyjaszewski, T. Kowalewski, *J. Am. Chem. Soc.* **2005**, *127*, 6918.
[62] S. H. Kim, M. J. Misner, T. Xu, M. Kimura, T. P. Russell, *Adv. Mater.* **2004**, *16*, 226.
[63] L. Rockford, Y. Liu, P. Mansky, T. P. Russell, M. Yoon, S. G. J. Mochrie, *Phys. Rev. Lett.* **1999**, *82*, 2602.
[64] S. O. Kim, H. H. Solak, M. P. Stoykovich, N. J. Ferrier, J. J. de Pablo, P. F. Nealey, *Nature* **2003**, *424*, 411.
[65] M. Stoykovich, M. Müller, S. O. Kim, H. H. Solak, E. W. Edward, J. J. De Pablo, P. F. Nealey, *Science* **2005**, *308*, 1442.
[66] J. Y. Cheng, C. T. Rettner, D. P. Sanders, H.-C. Kim, W. D. Hinsberg, *Adv. Mater.* **2008**, *20*, 3155.
[67] Y. Zhang, U. Wiesner, H. W. Spiess, *Macromolecules* **1995**, *28*, 778.
[68] U. Wiesner, "*Lecture Notes in Physics*", Vol. 532, Springer, Berlin/Heidelberg 1999, pp. 214.
[69] D. E. Angelescu, J. H. Waller, D. A. Adamson, P. Deshpandle, S. Y. Chou, R. A. Register, P. M. Chaikin, *Adv. Mater.* **2004**, *16*, 1736.
[70] Y. R. Hong, D. H. Adamson, P. M. Chaikin, R. A. Register, *Soft Matter* **2009**, *5*, 1687.
[71] H. J. Jung, J. Chang, Y. J. Park, S. J. Kang, B. Lotz, J. Huh, C. Park, *Macromolecules* **2009**, *42*, 4148.
[72] J. Zhang, Y. Han, *Chem. Soc. Rev.* **2010**, published online, 10.1039/b816231j.
[73] T. Morkved, M. Lu, A. M. Urbas, E. E. Ehrichs, H. M. Jaeger, P. Mansky, T. P. Russell, *Science* **1996**, *273*, 931.

[74] K. Schmidt, H. G. Schoberth, M. Ruppel, H. Zettl, H. Hänsel, T. M. Weiss, V. Urban, G. Krausch, A. Böker, *Nat. Mater.* **2008**, *7*, 142.
[75] V. Olszowka, V. Kuntermann, A. Böker, *Macromolecules* **2008**, *41*, 5515.
[76] S. Sakurai, *Polymer* **2008**, *49*, 2781.
[77] J. Peng, Y. Xuan, H. Wang, Y. Yang, B. Li, Y. Han, *J. Chem. Phys.* **2004**, *120*, 11163.
[78] J. Peng, Y. Wei, H. Wang, B. Li, Y. Han, *Macromol. Rapid Commun.* **2005**, *26*, 738.
[79] Y. Xuan, J. Peng, L. Cui, H. Wang, B. Li, Y. Han, *Macromolecules* **2004**, *37*, 7301.
[80] F. S. Bates, G. H. Fredrickson, *Phys. Today* **1999**, *52*, 32.
[81] W. Zheng, Z. G. Wang, *Macromolecules* **1996**, *28*, 7215.
[82] H. Elbs, C. Drummer, V. Abetz, G. Krausch, *Macromolecules* **2002**, *35*, 5570.
[83] C. Lou, W. Huang, Y. Han, C. Pan, *Macromol. Rapid. Commun.* **2009**, *30*, 515.
[84] C. Luo, W. Huang, Y. Han, *Macromol. Rapid Commun.* **2009**, *22*, **1917**.
[85] C. Luo, W. Huang, Y. Han, unpublished.
[86] J. Peng, Y. Xuan, H. Wang, Y. Yang, B. Li, Y. Han, *J. Chem. Phys.* **2004**, *120*, 11163.
[87] E. Han, K. O. Stuen, M. Leolukman, C. C. Liu, P. F. Nealey, P. Gopalan, *Macromolecules* **2009**, *42*, 4896.

DOI: 10.1002/marc.200900541